Appl. Phys. B 65, 235–243 (1997)

Applied Physics B Lasers and Optics

High-average-power diode-pumped femtosecond Cr:LiSAF lasers

D. Kopf[1], **K.J. Weingarten**[2], **G. Zhang**[1], **M. Moser**[3], **M.A. Emanuel**[4], **R.J. Beach**[4], **J.A. Skidmore**[4], **U. Keller**[1]

[1] Ultrafast Laser Physics Laboratory, Institute of Quantum Electronics, Swiss Federal Institute of Technology, ETH Hönggerberg, HPT, CH-8093 Zürich, Switzerland
(Fax: 011-41/633 10 59, E-mail: kopf@iqe.phys.ethz.ch, WWW: http://iqe.ethz.ch/ultrafast/Welcome.html)
[2] Time-Bandwidth Products AG, Technoparkstr. 1, CH-8005 Zürich, Switzerland
[3] Paul Scherrer Institute, PSI, Zürich, Switzerland
[4] Lawrence Livermore National Laboratory, P.O. Box 808, L-250, Livermore, California 94550, USA

Received: 27 February 1997/Revised version: 14 April 1997

Abstract. We achieve 0.5-W and 110-fs pulses from a diode-pumped mode locked Cr:LiSAF laser, pumped by a 1200-times diffraction-limited 0.9-cm-wide 15-W diode-laser array. Pulses as short as 50 fs at 0.34 W are obtained, and a continous-wave output power of 1.42 W. These high-power results are based on an optimized mode-matching technique for good pump beam to cavity mode overlap, combined with a specialized crystal size and cooling geometry. A semiconductor saturable absorber mirror (SESAM) with low insertion loss is used to start and stabilize the mode locking. Using this device has the advantage that the mode locking dynamics are decoupled from the cavity layout, which is important for the design of the high-power resonator. In comparison to this high-power approach, we obtain 125-mW, 60-fs, and 105-mW, 45-fs pulses from a standard diode-pumped femtosecond Cr:LiSAF laser using two 12-times diffraction-limited high-brightness 0.5-W, 100-μm pump diodes.

PACS: 42.55R; 42.60F; 42.60D

Diode pumping of ultrafast lasers has been one of the key technical advances in the field of all-solid-state lasers of the last few years. For femtosecond pulse generation, Cr:LiSAF [1] and related materials are attractive solid- state laser media because they are broadband and laser-diode-pumpable. However, the power levels typically obtained from standard diode-pumped mode locked femtosecond Cr:LiSAF lasers are on the order of 100 mW ([2–8] and Sect. 2.2). This paper discusses a novel diode-pumping approach for Cr:LiSAF and compares it with the standard setup. The experiments presented show that mode locked output power of 0.5 W is possible from a diode-pumped Cr:LiSAF laser Sect. 2.3, thus providing a potentially more compact and lower-cost replacement for Ti:sapphire lasers, which are usually pumped by Ar-ion or frequency-doubled Nd-doped solid-state lasers.

Our diode-pumping approach is based on optimized mode-matching (OMM) combined with a specialized crystal geometry for cooling. A strongly asymmetric pump beam inside the gain medium is matched to the cavity mode of similar size and ellipticity. This achieves the smallest possible beam cross-section in the medium at sufficiently small pump beam divergence across the absorption length, resulting in optimized small-signal gain. The experiment is based on a 1200-times (5-times) diffraction-limited pump beam in the tangential plane (sagittal direction) from a 0.9 cm wide 15-W diode-laser array. The tangential (sagittal) axis is also referred to as the slow (fast) axis, which corresponds to the different divergence of the pump diode array. We compare this approach with the previous, standard diode-pumping scheme based on lower-power, high-brightness pump diodes (Sect. 1.2). These earlier experiments were commonly based on a pump arrangement which uses, for example, two (or more) diode lasers with a beam quality about 12-times (1-times) the diffraction limit in the tangential (sagittal) direction.

The benefits of Cr:LiSAF, i.e. the broadband emission and the absorption around 670 nm for diode pumping, are accompanied by several difficulties summarized in Sect. 1.1 which resulted in limited output power in previous systems. In comparison, the related materials Cr:LiSGAF [9] and Cr:LiCAF [10] typically have not shown improved output power to date but may turn out to be attractive alternatives. To start and stabilize the mode locking, we use a low-loss semiconductor saturable absorber mirror (SESAM) [11–13], which simply replaces one of the flat cavity mirrors. Semiconductors are inherent intensity-dependent saturable absorbers, allowing for reasonably large flexibility in the cavity configuration, as opposed to Kerr-lens mode locking (KLM) [14–17], which requires more constraints on the cavity design. Using SESAMs allows more freedom to design the cavity following the guidelines for the high-power diode pumping, which would be very difficult if the Kerr-lens design constraints were also applied. To date, the SESAM-based Cr:LiSAF mode locking experiments [2, 3, 7, 18] have tended to show higher output power (i.e. as high as 125 mW [3]), whereas the KLM Cr:LiSAF [4–6, 8, 19] and Cr:LiSGAF [20] lasers have demonstrated shorter pulses.

Such compact, easy-to-use, turnkey femtosecond lasers are interesting for a number of applications. These lasers are useful as a research tool in physics, chemistry, and biology, where they support ultrafast time-resolved studies, pump probe characterizations, nonlinear optical experiments, and so on. They can be used as a pulse seed source for femtosecond optical parametric oscillators or high-power amplification systems, which are again used in research and nonlinear optics. Forthcoming applications are anticipated in the medical area [21], in two-photon microscopy [22, 23], and materials processing [24, 25], which could make femtosecond sources even more attractive.

In Sect. 1, we discuss standard and high-power diode-pumping approaches for continous-wave (cw) Cr:LiSAF lasers: compare the related materials Cr:LiSAF, Cr:LiSGAF, and Cr:LiCAF and summarize the standard diode-pump setup; and discuss the concept and experiment of the high-power diode-pumped cw Cr:LiSAF laser based on OMM. Sect. 2 describes the corresponding femtosecond cw mode locking results, which use the SESAM. We conclude in Sect. 3.

Table 1. Properties

		Cr:LiSAF	Cr:LiSGAF	Cr:LiCAF
Emission cross section ($\pi - pol$)	(10^{-20} cm^{-2})	4.8 [9]	3.3 [9]	1.3 [9]
Fluorescence lifetime	(μs)	67 [9]	88 [9]	170 [9]
Small-signal gain FOM	(10^{-22} cm$^{-2}\mu$s)	3.2	2.9	2.2
Critical temperature for upper-state lifetime quenching	(°C)	69 [27]		255 [27]
Intrinsinc slope efficiency	(%)	53 [9]	52 [9]	67 [9]
Thermal conductivity along *c*-axis (*a*-axis)	(W/mK)	3.3 (3.0) [28]	3.6 (3.4) [28]	5.14 (4.58) [28]
Thermal expansion coefficient along *c*-axis (*a*-axis)	(10^{-6} /°C)	−10 (25) [9]	0 (12) [9]	3.6 (22) [9]
Thermal dispersion dn/dT, along *c*-axis (*a*-axis)	(10^{-6} /°C)	−4.0 (−2.5) [31]		−4.6 (−4.2) [28]

1 Diode-pumping of cw Cr:LiSAF

1.1 Difficulties of Cr:LiSAF, Cr:LiSGAF, *and* Cr:LiCAF

Diode-pumped Cr:LiSAF is subject to the following difficulties which tend to limit the available output power. The gain of Cr:LiSAF [26] is relatively low compared with other diode- pumped laser media, e.g. 30 times less than that of Nd:YAG. Furthermore, Cr:LiSAF has poor thermal conductivity [9], about 10 times smaller than that of Ti:sapphire. Additionally, it exhibits upper-state lifetime quenching with a critical temperature of 67 °C [27] which results in a rapid decrease in gain at temperatures thereabove. Finally, the diode-laser pump beam quality is highly non-diffraction-limited at the multiple-watt power level, which calls for a short absorption length to improve the overlap to the laser mode (i.e. mode matching). However, the desired short absorption length results in an increased temperature rise at the pump spot and thus typically leads to a stronger decrease in gain due to upper-state lifetime quenching.

The related materials Cr:LiSGAF [9] and Cr:LiCAF [10] have not shown improved output power [20, 28] over Cr: LiSAF experiments to date. However, some works report that Cr:LiSGAF shows less upconversion and excited-state absorption [29, 30] and reduced thermal lensing [20] than Cr:LiSAF. However, to date the thermal properties of Cr:LiSGAF are not yet fully reported, and thus its thermal lensing cannot be compared with that of Cr:LiSAF. Fortunately, thermal lensing is not yet an issue in standard diode-pumped systems, nor was it critical in the high-power approach of Sect. 1.3 or Sect. 2.3. In Table 1 we give a listing of all known and relevant parameters of these laser materials. Upconversion in Cr:LiSAF [26] was found to limit the laser performance in Q-switched operation [29], but usually not in cw mode locking, where the excitation density is pinned at a several times lower level. The excitation density is further decreased due to the longer absorption length in the high-power experiment of Sect. 1.3 at equivalent pump intensity, which reduces upconversion to a negligible effect. Cr:LiCAF would be the best choice for the laser medium, provided the scatter losses [28] can be reduced to those of Cr:LiSAF or Cr:LiSGAF. Despite Cr:LiCAFs slightly smaller (1.5 times) small-signal gain compared with that of Cr:LiSAF/Cr:LiSGAF, the main advantages of Cr:LiCAF would be that the critical temperature for upper-state lifetime quenching is much higher (255 °C) [27] and the intrinsic slope efficiency 67 % [10] as compared with 53 % in Cr:LiSAF [1] and 52 % in Cr:LiSGAF [9]. Moreover, Cr:LiCAF was reported to show only a little thermal lensing compared with Cr:LiSAF [31], as experimentally verified in a flash-lamp-pumped rod [32].

1.2 Standard diode-pumping approach

The above difficulties are the main reasons standard diode-pumped Cr:LiSAF lasers have not yet shown more than approximately 230 mW output power in cw mode and 125 mW in mode locked operation (Sect. 2 and [3]). The "standard" diode-pumping approach, used in most previously reported Cr:LiSAF experiments [2–6, 18] was typically based on (at least) two high-brightness pump diodes, e.g. diodes emitting 400–500 mW from a 100 μm stripe width, or similar. This corresponds to a beam quality [33, 34] approximately 12 times the diffraction limit, corresponding to $M_x^2 \approx 12$ (x denotes the tangential or slow axis, y the sagittal or fast axis). We model the non-diffraction-limited beam propagation assuming a Gaussian beam with an effective wavelength M^2 times the optical wavelength [33]. In our experiment, we focus the diode laser pump light from such a 500-mW, 100-μm diode to a spot-size diameter of 70 μm × 60 μm at the position of the laser crystal (see pump-focusing optics in Fig. 1). Figure 2 shows the resulting beam profile at the position of the laser crystal, as measured with a moving-slit beam scan. The confocal parameter of the pump beam in the tangential plane is ≈ 0.5 mm. This is well matched to the absorption length $L = 0.5$ mm of the 3 %-doped Cr:LiSAF at $\lambda = 670$ nm pump wavelength, as required for mode matching

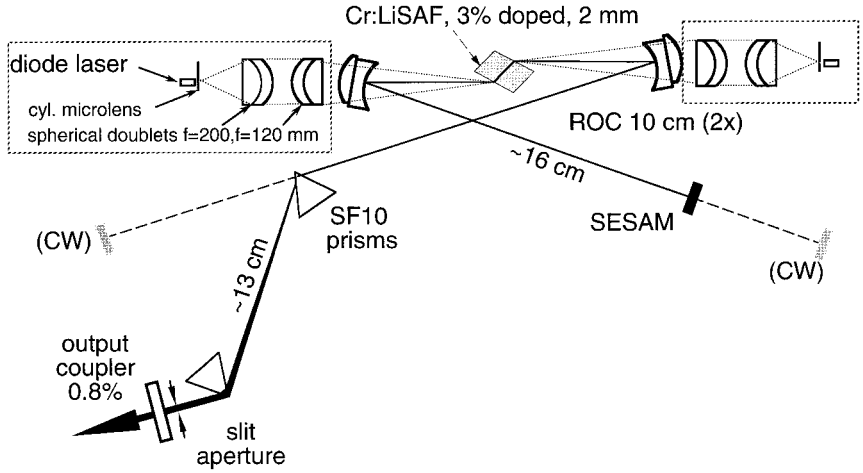

Fig. 1. Standard-diode-pumped femtosecond Cr:LiSAF resonator with a cavity repetition rate of 176 MHz. The SF10 prisms are Brewster-cut for minimum insertion loss. For cw operation (indicated by dashed lines), a high-reflector is used instead of the SESAM, and the prism pair is removed. ROC, radius of curvature; SESAM, semiconductor saturable absorber mirror

of the pump to the mode in the tangential plane (see next section). In the sagittal direction, the pump beam is diffraction-limited and assumes a focus of 50–60 μm diameter (Fig. 2). The cw cavity (Fig. 1 without the SESAM and the prism pair) has a resonator mode with a focus of 70 μm × 55 μm diameter in the laser medium which is reasonably well matched to the pump beam. The pump slightly overfills the mode in the tangential plane, since we have to take into account that the pump beam is stretched in the tangential plane by a factor of $n = 1.4$, refractive index, inside the medium due to the Brewster surfaces. In cw operation, a maximum output power of approximately 230 mW is typically obtained at a total absorbed pump power of 700 mW from the two pump diodes and a 1 % output coupler.

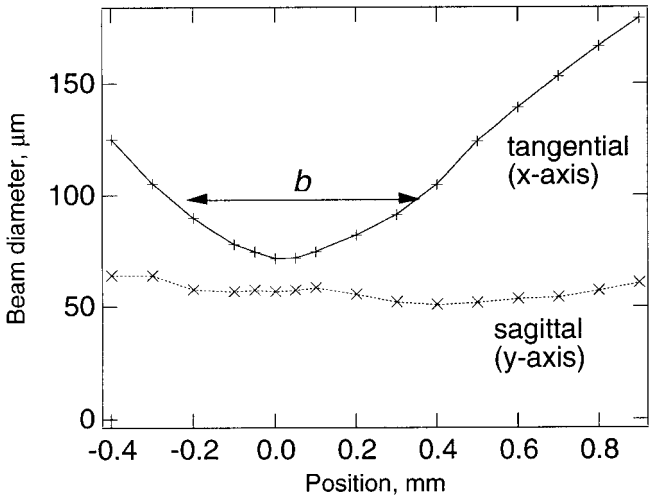

Fig. 2. Pump beam profile measured with a moving-slit beam scan at the position of the laser crystal in the standard diode-pumped Cr:LiSAF laser setup. The pump diode is a commercially available 500-mW, 100-μm red diode laser array with a 12-times diffraction limited beam in the tangential plane (i.e. $M_x^2 \approx 12$), and a diffraction-limited beam in the sagittal direction (i.e. $M_y^2 \approx 1$). The confocal parameter b of the pump beam is in good agreement with the absorption length of 0.5 mm. The sagittal beam profile has an uncritical divergence

1.3 High-power approach:(OMM) and cooling

The approach described in the previous section is only concerned about the tangential plane where the diode beam is non-diffraction-limited. Optimized mode- matching goes a step further and optimizes the overlap of pump beam and laser mode in both transverse directions, independently. This requires the ability to choose the waist in both the tangential plane and the sagittal direction for both the pump beam and the laser mode. The pump focusing requirement is governed by [35–37].

$$b_x = b_y = L\,, \tag{1}$$

where L is the Cr:LiSAF pump absorption length, b_x and b_y are the pump confocal parameters, given the pump waists w_x and w_y inside the laser crystal in the tangential plane (x) and the sagittal direction (y). Criterion (1) ensures that the pump beam will not significantly diverge over the dimension of the absorption length. Thus, the pump beam for typical diode-laser arrays with $M_x^2 \gg M_y^2 \cong 1$ is strongly asymmetric, because

$$w_{x,y}^2 = \frac{b_{x,y}\lambda M_{x,y}^2}{2\pi n}\,. \tag{2}$$

Equation (1) serves to achieve the smallest possible cross-sectional area of pump and mode over the entire absorption length. This optimizes the small-signal gain g_0 achieved in the gain medium. Since g_0 scales with the inverse of the cross-sectional area, the resulting small signal gain is [37]

$$g_0 \propto \frac{P}{\left(L\sqrt{M_x^2 M_y^2}\right)}\,, \tag{3}$$

where P is the total absorbed pump power. For typical high-power diode-laser arrays, the pump beam quality factors are $M_x^2 \gg 1$ and $M_y^2 \cong 1$, and the beam quality in x scales linearly with the emitted power $M_x^2 \propto P$. This is confirmed by the argument that diode arrays were shown to be extended to wider arrays and higher power while keeping the brightness

constant, i.e. both the divergence and the emitted power per unit stripe width [38, 39]. Simplifying (3) we obtain a figure-of-merit (FOM) for OMM-based diode pumping [37]

$$\mathrm{FOM} \equiv \frac{p}{\sqrt{M_x^2 M_y^2}} \propto \sqrt{M_x^2} \propto \sqrt{P}\,, \tag{4}$$

The scaling of (4) assumes a constant absorption length L. This FOM tells us that high-power diode-laser arrays can pump solid-state laser media without trading off small-signal gain despite the highly non-diffraction-limited beam, provided that OMM is applied. High-power diode arrays can even produce higher small-signal gain than diode lasers of equivalent brightness but lower power. However, this scaling can be traded off by thermal effects, which were not taken into account in the FOM of (4).

For the case of Cr:LiSAF, thermal issues need to be taken into account because of Cr:LiSAF's thermal difficulties (Sect. 1.1). Therefore, we choose a specialized crystal size and cooling geometry (Fig. 3a) which reduce the temperature rise at the pump spot. A vertically thin (1 mm) Cr:LiSAF crystal and a relatively long absorption length (4 mm) establish a mainly one-dimensional heat flow. The resulting temperature rise is then only a few tens of degrees centigrade even at several watts of deposited heat, as numerical heat flow simulations show [37]. Assuming homogeneous heat deposition over the absorption length and two-dimensional heat flow in the x-y-plane, we can calculate the resulting temperature profile along the x-and y-direction (Fig. 3b) which shows a maximum temperature rise of 35 °C at a total deposited heat of 3 W, which approximately corresponds to the experimental conditions of Fig. 4a. Figure 3c confirms the assumption for a mainly one-dimensional heat flow. The maximum temperature rise is calculated as the pump spot diameter Δx in the x-direction (Fig. 3a) is increased while keeping a constant pump intensity at the pump spot. This results in a linear increase of pump power. For spot widths larger than 2 mm, we observe predominantly one-dimensional heat flow which results in no significant increase in temperature rise despite the increased total amount of deposited heat.

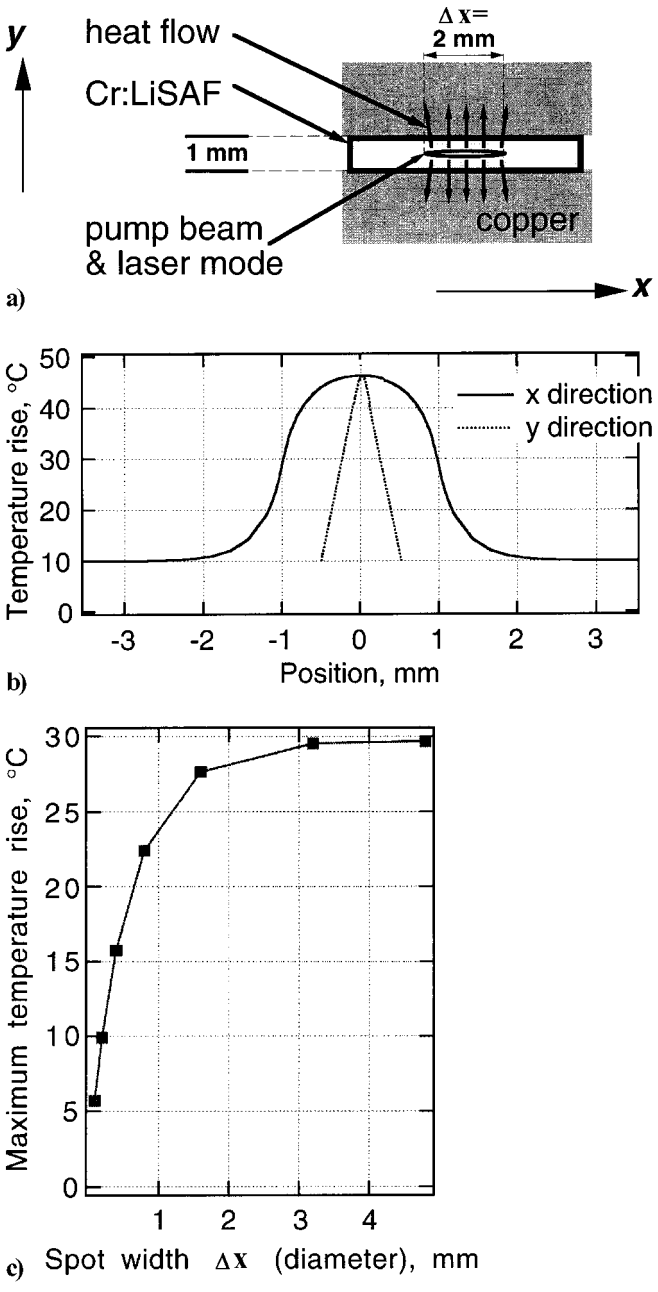

Fig. 3. a Schematic cross-sectional view of the laser crystal pumped by a strongly asymmetric diode laser beam. The crystal geometry causes a mainly one-dimensional heat flow to the copper heat sinks. **b** Calculated temperature profile for 3 W deposited heat. **c** Calculated maximum temperature rise with increased pump spot width Δx at constant pump intensity, i.e. increased total pump power

For the case of Cr:LiSAF, thermal issues need to be taken into account because of Cr:LiSAF's thermal difficulties (Sect. 1.1). Therefore, we choose a specialized crystal size and cooling geometry (Fig. 3a) which reduce the temperature rise at the pump spot. A vertically thin (1 mm) Cr:LiSAF crystal and a relatively long absorption length (4 mm) establish a mainly one-dimensional heat flow. The resulting temperature rise is then only a few tens of degrees centigrade even at several watts of deposited heat, as numerical heat flow simulations show [37]. Assuming homogeneous heat deposition over the absorption length and two-dimensional heat flow in the x-y-plane, we can calculate the resulting temperature profile along the x-and y-direction (Fig. 3b) which shows a maximum temperature rise of 35 °C at a total deposited heat of 3 W, which approximately corresponds to the experimental conditions of Fig. 4a. Figure 3c confirms the assumption for a mainly one-dimensional heat flow. The maximum temperature rise is calculated as the pump spot diameter Δx in the x-direction (Fig. 3a) is increased while keeping a constant pump intensity at the pump spot. This results in a linear increase of pump power. For spot widths larger than 2 mm, we observe predominantly one-dimensional heat flow which results in no significant increase in temperature rise despite the increased total amount of deposited heat.

The first experiments tended to optimize the pump-to-mode overlap according to this OMM and were demonstrated with either Nd:YAG or Nd:YLF as the laser medium [40–42]. However, simpler diode-pumping techniques such as side pumping provide enough small-signal gain for efficiently achieving high average powers in these materials. For Cr:LiSAF, which has considerably lower gain, OMM remains an important technique in achieving efficient diode pumping.

The high-power Cr:LiSAF laser experiment (Fig. 4) uses as pump source a $W = 0.9$ cm wide diode-laser array with a maximum emitted power of 15 W at $\lambda = 690$ nm [38, 39]. The power density is about twice as low as that of the commercially available 500-mW diode used in Sect. 1, thus indicating that long-term reliability may be expected [43]. The diode beam has a tangential beam divergence of $\theta_x = \pm 3.5°$, and thus the beam is

$$M_x^2 = \pi \frac{W}{2} \cdot \frac{\theta_x}{\lambda} \cong 1200\,, \tag{5}$$

times diffraction-limited in the tangential plane. In the sagittal direction, the diode beam is strongly divergent ("fast" or y-axis) but diffraction limited. After the cylindrical microlens, which collects the light in the fast direction, the beam was measured to be 5 times diffraction-limited. This is attributed to a slight misalignment of the microlens.

It is very difficult to keep the microlens aligned across the entire diode stripe width, which results in varying vertical exit angles across the stripe. To reduce this beam distortion, we split the diode pump beam into two parts (Fig. 4b). Additionally, each half beam has an M_x^2 reduced by a factor of 2. The pump-focusing optics further consist of two cylindrical lenses followed by a spherical doublet ($f = 80$ mm) and a meniscus

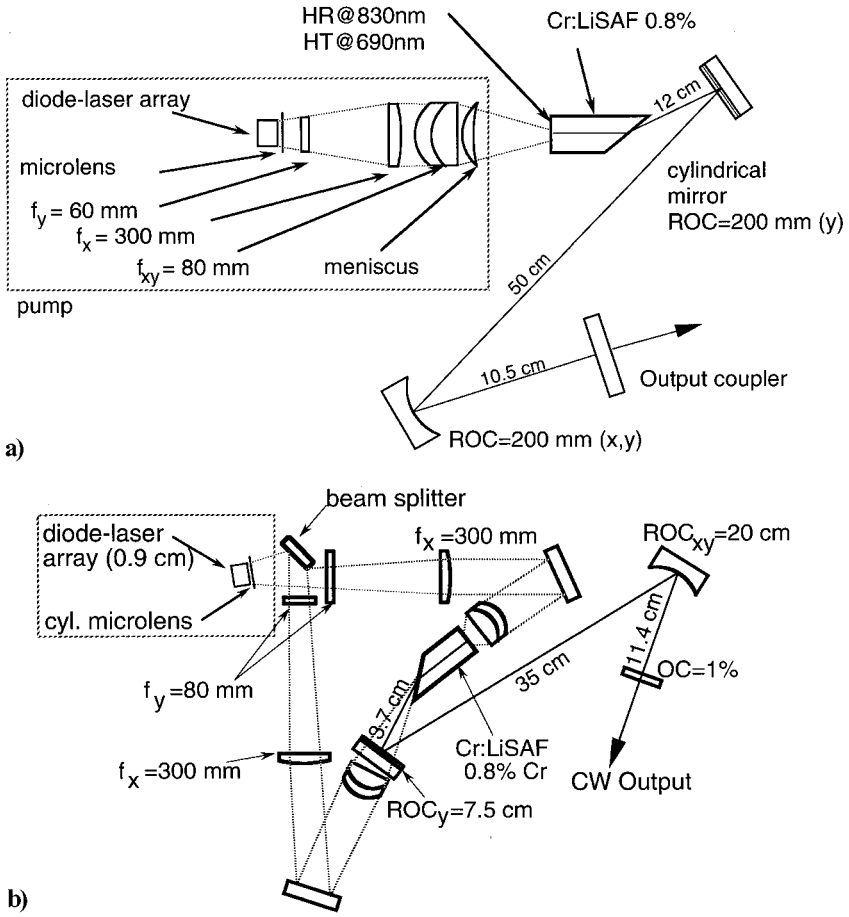

Fig. 4. a High-power cw Cr:LiSAF cavity pumped by a 0.9-cm-wide 15-W diode-laser array. **b** By splitting the pump beam in two beams we can reduce M_x^2 by a factor of 2

lens (Melles Griot, 01LMP003, f= 100 mm, 50 mm diameter). The beam is imaged into the crystal to a spot-size diameter of less than 1.25 mm × 100 μm over the absorption length of 4 mm. Figure 5 shows the beam profiles in x and y at the position of the laser crystal, and that they are in reasonable agreement with the OMM requirements of (1). The strongly asymmetric pump beam, as required by (2), is due to the strongly asymmetric pump beam quality factors $M_x^2 \gg M_y^2$.

The cw laser (Fig. 4b) has a cavity mode of asymmetry and size ($\approx 1\,\text{mm} \times 80\,\mu\text{m}$ diameter) similar to that of the pump beam in the Cr:LiSAF crystal, such that they overlap in the gain medium over the entire absorption length L according to OMM. This strongly asymmetric mode is achieved by the use of a cylindrical cavity mirror with a vertical radius of curvature $\text{ROC}_y = 75$ mm in Fig. 4b. The rest of the cw cavity consists of a curved folding mirror and a flat 1 % output coupler; the cavity mode is relatively round with an aspect ratio less than 2 : 1.

The results of the cw experiment using the Cr:LiSAF laser cavity shown in Fig. 4b are shown in Fig. 6. We achieve a maximum cw output power of 1.42 W at a total absorbed pump power of 9.3 W. Slightly lower cw output power was achieved with the Cr:LiSAF cavity shown in Fig. 4a [37]. The output power as a function of absorbed pump power (Fig. 6) shows no significant saturation, as expected from the temperature profile calculations (Fig. 3). The output beam quality is near-diffraction-limited with an $M_x^2 = 1.7$ at 1.2 W and $M_x^2 = 2.8$ at 1.4 W output power. In the sagittal plane the output beam was diffraction-limited ($M_y^2 \approx 1$). We anticipate that further optimization of the pump focusing will lead to higher output powers.

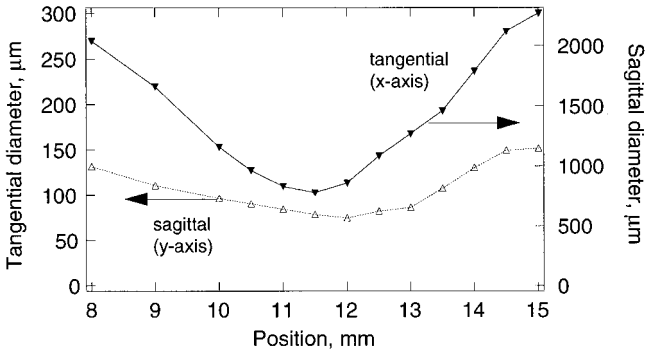

Fig. 5. Pump beam profile of splitted pump beam (i.e. half-beam) taken at the position of the laser crystal in the high-power diode-pumped Cr:LiSAF laser setup (Fig. 4b). The pump diode is a 15-W, 0.9-cm-wide red diode-laser array with a 1200-times diffraction-limited beam in the tangential plane and a diffraction-limited beam in the sagittal direction. The confocal parameter of the pump beam is in good agreement with the absorption length of 4 mm in both transverse directions $x$and y, simultaneously, as required for OMM

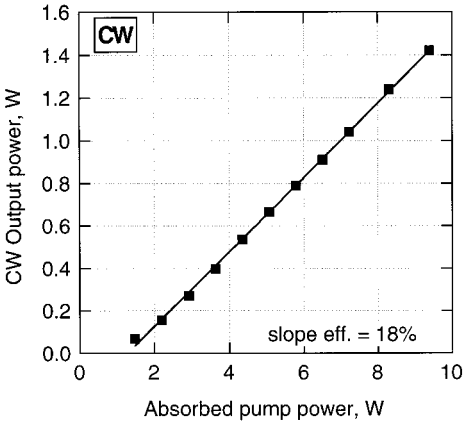

Fig. 6. Continous-wave output power obtained from the diode-pumped Cr:LiSAF laser (Fig. 4b) as a function of absorbed pump power

2 Diode-pumped femtosecond Cr:LiSAF experiments

2.1 Semiconductor saturable absorber mirrors

We pioneered and established semiconductor saturable absorber mirrors [11, 13] for passively mode-locked solid-state lasers. The first device used in a diode-pumped Cr:LiSAF laser demonstrated picosecond pulses [44] with a resonant passive mode-locking arrangement (RPM) [45, 46], and later an intracavity SESAM also generated sub-picosecond pulses [44], but at very low average powers. In 1994, we demonstrated considerably improved output power, using a high-finesse A-FPSA as the SESAM to start and stabilize the mode-locking. We obtained $\approx$ 100-fs pulses with 50 mW of average output power [2, 47]. Shortly following these results, diode-pumped Cr:LiSAF lasers based on KLM showed the first femtosecond mode-locking results [48], despite the low nonlinear refractive index of Cr:LiSAF compared with Ti:sapphire. In comparison, the SESAM-based systems generally generated self-starting pulsing, whereas the KLM lasers typically were not self-starting (except [6]). Further improved results include self- starting pulses of 45 fs at 60 mW [3, 49] and 60 fs at 125 mW [3] from standard systems (next section). Other groups have reported on diode-pumped femtosecond results such as 100 fs, 11 mW [18] and 70 fs, 100 mW [7], also employing a SESAM, then 40 fs at 70 mW [5], 70 fs at 50 mW [6], 100 fs at 35 mW [20], and 94 fs at 50 mW [8], all based on KLM. The shortest pulses were also obtained from a KLM diode-pumped Cr:LiSAF with $\approx$ 20-fs pulses at a few mW output power [4, 50].

The SESAM used throughout this paper is a broadband low-finesse A-FPSA [3] with the structure shown in Fig. 7. The Bragg mirror (R> 99.5 %) and the semiconductor-to-air interface (R$\approx$ 31 %) are the two dominant reflecting surfaces which define the low-finesse Fabry–Perot. In the earlier designs, we evaporated on top of the structure a highly reflecting mirror (R> 95 %) which define a high-finesse Fabry–Perot. In this work, a 15 nm thick GaAs absorber quantum well with a bandgap wavelength of approximately 860 nm is positioned within a half-wavelength AlAs spacer layer (Fig. 7) which is transparent for the laser wavelength. The total thickness of a half-wavelength (optical thickness $\overline{n}d = \lambda/2$) corresponds to the antiresonance condition of the Fabry–Perot structure. Underneath is an MOCVD-grown Bragg mirror with a center wavelength of 850 nm. On top of the whole structure is a 5-nm-thick GaAs cap layer, which avoids oxidation of the underlying AlAs layer to air. The absorber layer is low-temperature (400 °C) MBE-grown, which broadens the absorption edge. Additionally, the position of the absorber layer is chosen in a way that the standing wave intensity is smaller for shorter wavelengths, where the material-given absorption of GaAs is stronger. This results in a relatively flat wavelength dependence of the low-intensity reflectivity of the structure [3], which is approximately 98.5 %±0.7 % across a wavelength range of 50 nm (Fig. 9). The low insertion loss is important to achieve high average output power levels, and the relatively small variation in reflectivity allows broad wavelength tunability. This is significant for Cr:LiSAF as the laser medium because of its low gain.

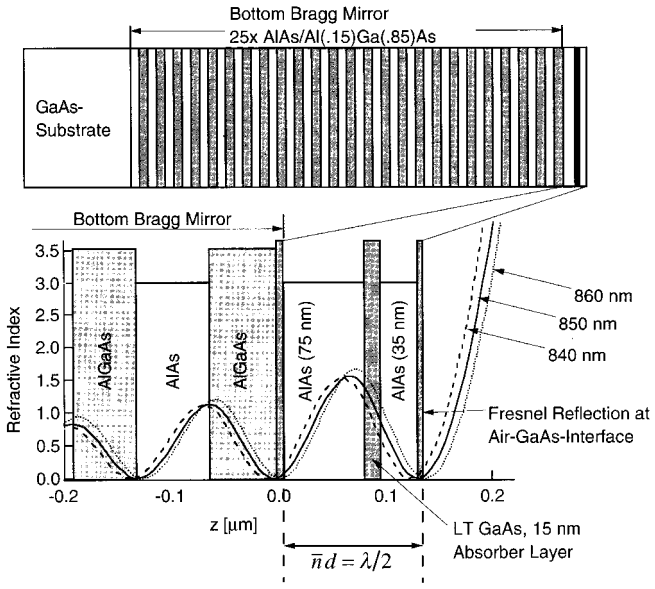

Fig. 7. Semiconductor saturable absorber mirror (SESAM) used throughout this paper. The structure is a low-finesse antiresonant Fabry–Perot saturable absorber (A-FPSA) which is optimized for broad wavelength tunability [3]. *Bottom*: Expanded view of the top layers of the structure. The standing wave patterns of the three wavelengths are plotted with equivalent intensity incident on the device. The two AlAs spacer layers and the GaAs saturable absorber layer (plus the two cap layers) have a total thickness of a half wave at 850 nm, which corresponds to antiresonance. *Top*: Whole structure of the SESAM including the Bragg mirror, on top of which the spacer layers, the saturable absorber layer, and the cap layer are grown. LT, low-temperature grown; *z*, position vertical to sample surface

The nonlinear reflectivity of the SESAM is due to absorption bleaching at high pulse energy densities. In our SESAM, we measured a fast time constant of $\approx$ 400 fs, and a slow time constant of several picoseconds (Fig. 8a) in a standard noncollinear degenerate pump-probe measurement using 100-fs pulses from a Ti:sapphire laser. These measurements were done with excitation levels slightly below the saturation fluence, and at the three wavelengths 830, 845, and 862 nm, with similar results at all wavelengths. We determined a saturation fluence of 160 μJ/cm^2 at 830 nm (Fig. 8b) for the SESAM which does not significantly change at other wavelengths. A theoretical fit in Fig. 8b is based on traveling–wave rate equations [12] and determines a maximum modulation depth of 1.4 % and a nonsaturable loss of 1 %. The bleached carriers recover on a time scale which can be varied by the low-temperature MBE growth.

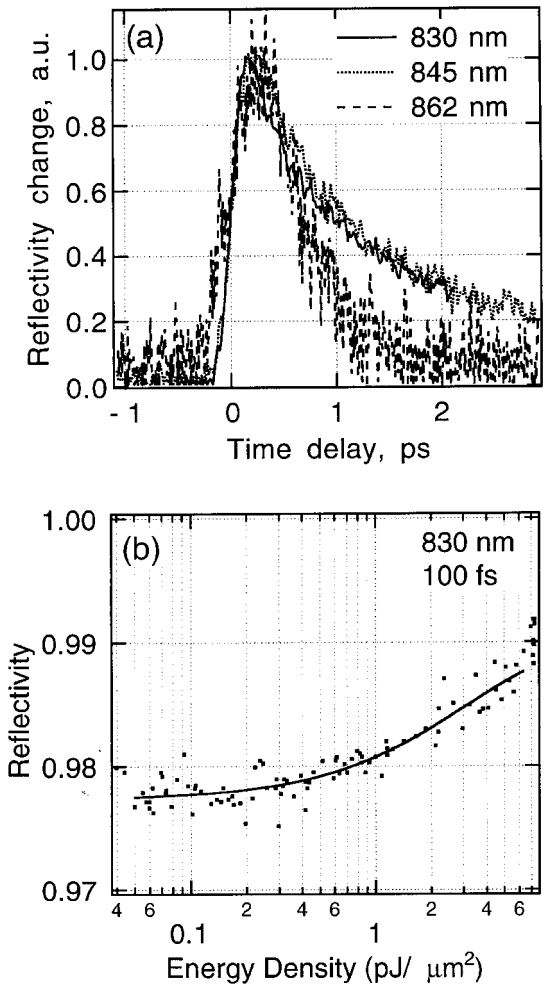

Fig. 8. a Pump probe measurements indicating the impulse response of the SESAM of Fig. 7 The three wavelengths show similar behavior. **b** Measured nonlinear reflectivity of the SESAM as a function of incident pulse energy density. The data are fitted assuming a saturation fluence $E_{sat} = 160\,\mu J/cm^2$ [12]

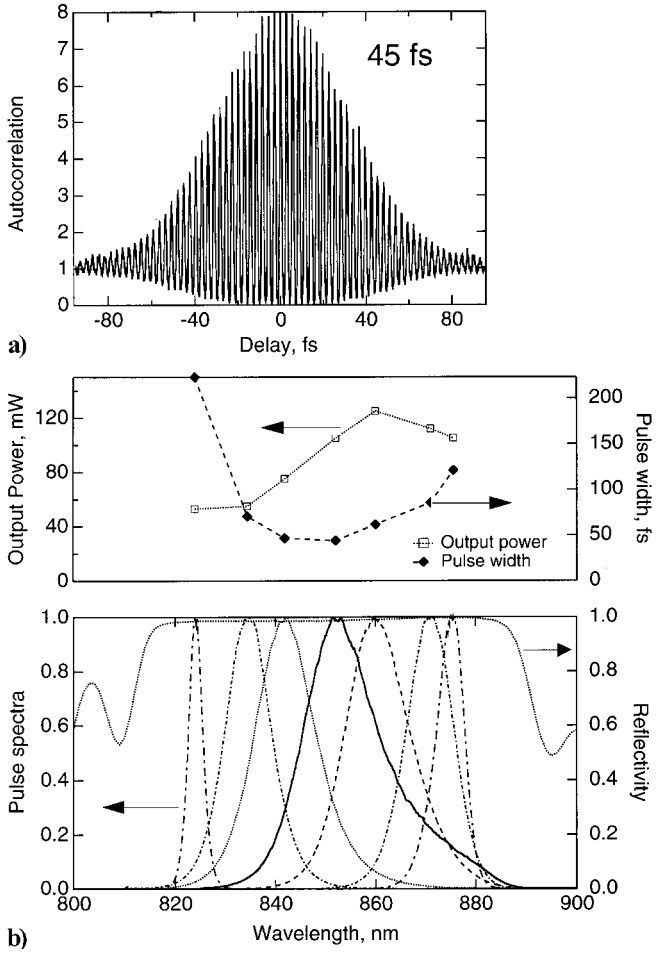

Fig. 9. a Interferometric autocorrelation measurement of the shortest pulse (45 fs, 105 mW) obtained from the standard diode-pumped Cr:LiSAF laser. The time bandwidth product is 0.31. **b** *Lower graph*: Reflectivity of the SESAM used in the experiments (dotted curve, right scale). The constant reflectivity and low loss across more than 50 nm allows for tunability of self-starting femtosecond generation, as the various pulse spectra show (left scale). *Upper graph*: Measured output power and pulse duration corresponding to the pulse spectra in the lower graph. The highest output power obtained is 125 mW at a pulse duration of 60 fs

2.2 Standard diode-pumped femtosecond Cr*:LiSAF laser*

The standard mode-locked Cr:LiSAF configuration (Fig. 1) uses the same pump scheme as that of Sect. 1.2. The cavity consists of two curved folding mirrors (radius of curvature ROC= 10 cm spherical), a 13 cm-long SF10 prism sequence followed by a flat 0.8 % output coupler, and the SESAM described in the previous section at the other end of the cavity. The distance between the two curved laser mirrors is 12.6 mm, which results in a laser mode of $100\,\mu m \times 110\,\mu m$ diameter on the SESAM. The mode waist at the laser crystal is the same as in the cw experiment of Sect. 1.2.

Figure 9a shows the shortest pulses with 45-fs duration obtained from this laser at an average output power of 105 mW (absorbed pump power, 700 mW). The highest average output power obtained is 125 mW with 60-fs pulses at a slightly shifted wavelength (Fig. 9b). This is the highest reported output power from a diode-pumped femtosecond Cr:LiSAF laser, except for the results of Sect. 2.3, where we have used a different pump approach. We could tune the laser wavelength over a range of more than 50 nm, due to the constant reflectivity and low loss of the SESAM across this range. Over the total wavelength range, self-starting femtosecond mode locking was obtained (Fig. 8b). During steady-state pulsing, the pulse energy density incident on the SESAM is $\approx 800\,\mu J/cm^2$ which is about 5 times the saturation fluence of the SESAM (see Sect. 1), thus causing strong absorption bleaching.

2.3 High-power diode-pumped femtosecond Cr*:LiSAF laser based on OMM*

For mode-locked operation, we extend the cw cavity of Sect. 1.3 to include the SESAM and a prism sequence for dispersion compensation (Fig. 10). This does not significantly change the laser mode in the gain medium, and thus provides the same OMM as in the cw case. The cavity is terminated by the SESAM of Sect. 2.1 where the laser mode size diameter is $300\,\mu m \times 540\,\mu m$. This results in a pulse energy density of $\approx 330\,\mu J/cm^2$ incident on the SESAM (assuming

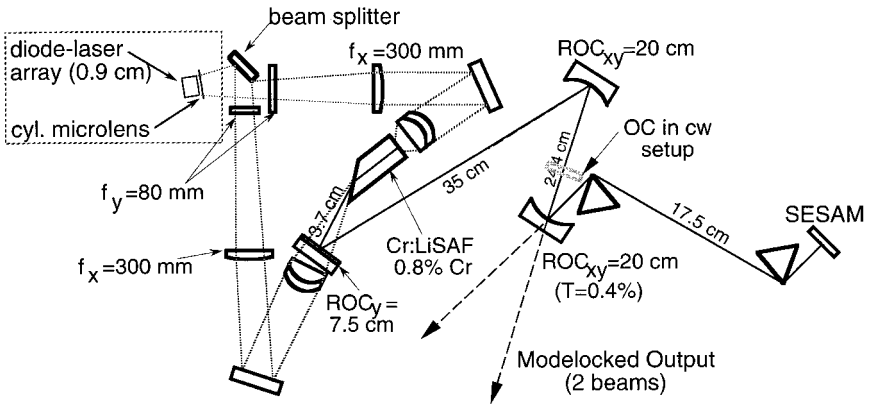

Fig. 10. High-power femtosecond Cr:LiSAF cavity pumped by a 15-W diode-laser array. The cw cavity of Fig. 4 is extended in such a way that a prism sequence and the SESAM for mode-locked operation are included. The pump optics stays unchanged. The cavity mode dimension inside the laser crystal remains virtually unchanged in comparison with the cw setup of Fig. 4. a knife edge is inserted to avoid higher spatial modes and ensure stable mode-locked operation

500 mW output power), which corresponds to twice the saturation fluence of the SESAM. The spot size on the SESAM is the only parameter that the cavity design has to take into account. Therefore, the cavity design is merely subject to the requirements of OMM (Sect. 1.3) but not, for example, to the additional constraints of KLM. The cavity repetition rate is 150 MHz. One of the curved turning mirrors (R= 99.6 %) serves as an 0.8 % output coupler, which results in two output beams. A single output beam carrying the full output power could be obtained if the flat side of the laser crystal were chosen to be the 0.8 % output coupler instead of the curved mirror. This would cause no changes to the cavity mode and only minor changes to the pump optics, which would then have to include a dichroic beam splitter to separate the output from the pump.

The modelocking experiments are shown in Fig. 11. We generate self-starting 110-fs pulses at a total output power of 500 mW (split between two 250-mW beams) at 8.3 W absorbed pump power, and self-starting 50-fs pulses at a total of 340 mW at 6.4 W absorbed pump. A knife edge was inserted into the beam (Fig. 10) to suppress higher order spatial modes and to obtain stable pulsing. This was also verified on a microwave spectrum analyzer monitoring the output signal on a photodiode. The center wavelength is at $\approx$ 875 nm.

2.4 Modelocking mechanism

Soliton mode-locking [51–53] is assumed to be the dominant mode-locking mechanism in our SESAM-based femtosecond lasers. The cavity was operated close to the middle of the stability regime without any critical cavity alignment necessary for KLM. Stable femtosecond pulse generation can be achieved with a relatively weak (i.e.< 1 %) nonlinear reflectivity due to semiconductor saturable absorption, provided that SPM and GVD are the dominant pulse-shaping effects. Additionally, the absorber recovery time may be approximately 10 times slower than the steady-state pulse duration (depending on the actual amount of SPM and GVD), as verified in [52]. Therefore, this SESAM can be used to generate pulses with durations down to the tens-of-femtoseconds regime.

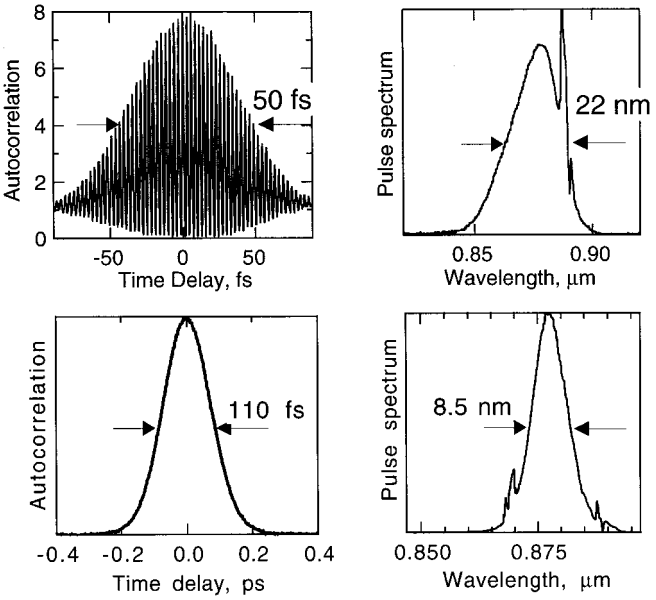

Fig. 11. Mode-locking results of high-power diode-pumped femtosecond Cr:LiSAF laser. *Upper graphs*: The shortest pulses obtained are self-starting 50-fs pulses at an output power of 340 mW, measured with an interferometric autocorrelation (left) and the spectrum (right). *Lower graphs*: Noncollinear autocorrelation and spectrum of self-starting 110-fs pulses at a total output power of 500 mW

3 Conclusion

We demonstrate 125-mW, 60-fs and 105-mW, 45-fs pulses from a standard diode-pumped Cr:LiSAF laser based on a SESAM which is optimized for low insertion loss. With a diode-pumping configuration utilizing OMM and a specialized crystal geometry for cooling, we show that we can produce 1.4 W cw and 0.5 W mode-locked output power from a diode-pumped Cr:LiSAF laser. We generate 0.5 W of 110-fs pulses and 0.34 W of 50-fs pulses started by the SESAM. We pump the Cr:LiSAF laser medium with a 0.9-cm-wide high-power diode-laser array which emits a 1200-times diffraction-limited beam in the tangential plane. The technique of OMM gives guidelines for the pump-focusing and cavity mode parameters in the crystal for optimum small-signal gain. The use

of the SESAM as the mode-locking element, in contrast to KLM, facilitates the design of the cavity with respect to the OMM requirements because the mode-locking dynamics are decoupled from the cavity layout. We think that these laser results show that a compact and cost-effective replacement for Ti:sapphire lasers is feasible without trading off output power.

Acknowledgements. This work was supported by the Swiss National Science Fund.

References

1. S.A. Payne, L.L. Chase, L.K. Smith, W.L. Kway, H. Newkirk: J. Appl. Phys., **66**, 1051 (1989)
2. D. Kopf, K.J. Weingarten, L. Brovelli, M. Kamp, U. Keller: Opt. Lett., **19**, 2143 (1994)
3. D. Kopf, A. Prasad, G. Zhang, M. Moser, U. Keller: Opt. Lett., **22**, 621 (1997)
4. M.J.P. Dymott, A.I. Ferguson: Opt. Lett., **20**,1157 (1995)
5. R. Mellish, N.P. Barry, S.C.W. Hyde, R. Jones, P.M.W. French, J.R. Taylor, C.J. v.d. Poel, A. Valster: Opt. Lett., **20**, 2312 (1995)
6. F. Falcoz, F. Balembois, P. Georges, A. Brun: Opt. Lett., **20**, 1874 (1995)
7. S. Tsuda, W.H. Knox, S.T. Cundiff: Appl. Phys Lett., **69**, 1538 (1996)
8. A. Robertson, R. Knappe, R. Wallenstein: J. Opt. Soc. Am. B, **14**, 672 (1997)
9. L.K. Smith, S.A. Payne, W.L. Kway, L.L. Chase, B.H.T. Chai: IEEE J.**28**, 2612 (1992)
10. S.A. Payne, L.L. Chase, H.W. Newkirk, L.K. Smith, W.F. Krupke: IEEE J. **24**, 2243 (1988)
11. U. Keller, D.A. B. Miller, G.D. Boyd, T.H. Chiu, J.F. Ferguson, M.T. Asom: Optics Lett., **17**, 505 (1992)
12. L.R. Brovelli, U. Keller, T.H. Chiu: J. Optic. Soc. Am. B, **12**, 311 (1995)
13. U. Keller, K.J. Weingarten, F.X. Kärtner, D. Kopf, B. Braun, I.D. Jung, R. Fluck, C. Hönninger, N. Matuschek, J. Aus der Au: IEEE JSTQE, **2**, 435 (1996)
14. D.E. Spence, P.N. Kean, W. Sibbett: Opt. Lett., **16**, 42 (1991)
15. U. Keller, G.W. 'tHooft, W.H. Knox, J.E. Cunningham: Opt. Lett., **16**, 1022 (1991)
16. D.K. Negus, L. Spinelli, N. Goldblatt, G. Feugnet: *In Advanced Solid-State Lasers*, ed. by G. Dubé, L. Chase; Vol. 10 (Optical Society of America, Washington DC, 1991) p. 120
17. F. Salin, J. Squier, M. Piché: Opt. Lett., **16**, 1674 (1991)
18. S. Tsuda, W.H. Knox, E.A. d. Souza, W.Y. Jan, J.E. Cunningham: Opt. Lett., **20** 1406 (1995)
19. P.M. Mellish, P.M.W. French, J.R. Taylor, P.J. Delfyett, L.T. Florez: Electron. Lett., **30** 223 (1994)
20. V.P. Yanovsky, F.W. Wise, A. Cassanho, H.P. Jenssen: Opt. Lett., **20**, 1304 (1995)
21. F.H. Loesel, P. Brockhaus, J.P. Fischer, M.H. Goetz, M. Tewes, M. Niemz, F. Noack, J.F. Bille: *"Conference on Lasers and Electro-optics"* (1994), Paper CWN2
22. W. Denk, J. Strickler, W.W. Webb: Science, **248**, 73 (1990)
23. C. Xu, W.W. Webb: J. Opt. Soc. Am. B, **13**, 481 (1996)
24. X. Liu, D. Du, A.-C. Tien, G. Mourou: *Conference on Lasers and Electro-Optics* (1996), Paper CThH2
25. C. Momma, S. Nolte, B. Chichkov, F.v. Alvensleben, A. Tünnermann: *Conference on Lasers and Electro-Optics* (1996), Paper CWE3
26. S.A. Payne, L.K. Smith, R.J. Beach, B.H.T. Chai, J.H. Tassano, L.D. DeLoach, W.L. Kway, R.W. Solarz, W.F. Krupke, Appl. Opt., **33**, 5526 (1994)
27. M. Stalder, M. Bass, B.H.T. Chai: J. Opt. Soc. Am. B, **9**, 2271 (1992)
28. A. Cassanho, V.K. Castillo, G.J. Quarles, H.P. Jenssen, S. Buchter, A. Bustamente, D. Hagan: *Conference on Lasers and Electro-Optics* (1996), Paper MJ3
29. F. Falcoz, K. Kerboull, F. Druon, F. Balembois, P. Georges, A. Brun: Opt. Lett., **21**, 1253 (1996)
30. E. Sorokin, I.T. Sorokina, E. Wintner, A. Cassanho, H.P. Jenssen: *Advanced Solid-State Lasers* (1997), Paper MB12
31. S.A. Payne, W.F. Krupke, L.K. Smith, W.L. Kway, L.D. DeLoach, J.B. Tassano: IEEE J. QE-**28**, 1188 (1992)
32. L.L. Chase, S.A. Payne, R.S. Hughes, B.W. Woods, L.E. Davis: In *Advanced Solid-State Lasers*, ed. by H.P.J. a.G. Dubés: OSA Proceedings (Optical Society of America, Washington DC 1990), pp. 83–85
33. M.W. Sasnett: *In the Physics and Technology of Laser Resonators*, ed. by D.R. Hall, P.E. Jackson (Adam Hilger, New York 1989) p. 132
34. T.F. Johnston: *Laser Focus World*, 1990, May
35. T.Y. Fan, A. Sanchez:IEEE J.QE-**26**, 311 (1990)
36. D. Kopf, J. Aus der Au, U. Keller, G.L. Bona, P. Roentgen: Opt. Lett. **20**, 1782 (1995)
37. D. Kopf, U. Keller, M.A. Emanuel, R.J. Beach, J.A. Skidmore: Opt. Lett., **22**, 99 (1997)
38. M.A. Emanuel, R.J. Beach, J.A. Skidmore, D. Hudson, W.J. Benett, B.L Freitas, N.W. Carlson: *Conference on Lasers and Electro-Optics*, (1994), Paper CMH2
39. J.A. Skidmore, M.A. Emanuel, R.J. Beach, W.J. Benett, B.L. Freitas, N.W. Carlson, R.W. Solarz: Appl. Phys. Lett., **66**, 1163 (1995)
40. D.C. Shannon, R.W. Wallace: Opt. Let, **16**, 318 (1991)
41. F. Krausz, J. Zehetner, T. Brabec, E. Wintner: Opt. Lett., **16**, 1496 (1991)
42. J. Zehetner, C. Spielmann, F. Krausz, E. Wintner: *In Advanced Solid-State Lasers*, ed. by L.L. Chase, A.A. Pinto, Vol. 13 of OSA Proceedings Series (Optical Society of America, Washington DC, 1992), pp. 215-218
43. The emitted power of 15 W from 0.9 cm stripe width corresponds to 2.4 mW/μm power density, taking into account the 70 % fill factor. In comparison, the commercially available 500-mW, 100-μm red diode lasers have a power density of 5 mW/μm. The fact that the diode-laser array consists of numerous diode lasers next to each other on the same chip should not result in increased heating, since the diode array is mounted on a silicon microchannel cooling plate. This provides efficient heat removal to the water coolant.
44. P.M.W. French, R. Mellish, J.R. Taylor: Opt. Lett., **18**, 1934 (1993)
45. U. Keller, W.H. Knox, H. Roskos: Opt. Lett., **15**, 1377 (1990)
46. U. Keller, T.H. Chiu: IEEE J.Quantum Electron, **28**, 1710 (1992)
47. D. Kopf, K.J. Weingarten, L. Brovelli, M. Kamp, U. Keller: *Conference on Lasers and Electro-Optics*, (1994) Paper CPD22
48. J.R. Lincoln, M.J.P. Dymott, A.I. Ferguson: Opt. Lett., **19**, 634 (1994)
49. D. Kopf, K.J. Weingarten, L.R. Brovelli, M. Kamp, U. Keller: *Conference on Lasers and Electro-optics*, (1995) Paper CWM2
50. M.J.P. Dymott, A.I. Ferguson: *Conference on Lasers and Electro-optics*, (1995), Paper CWM1
51. F.X. Kärtner, U. Keller: Opt. Lett., **20**, 16 (1995)
52. I.D. Jung, F.X. Kärtner, L.R. Brovelli, M. Kamp, U. Keller: Opt. Lett., **20**, 1892 (1995)
53. F.X. Kärtner, I.D. Jung, U. Keller, I. Paper:, IEEE JSTQE, **2**, 540 (1996)